HHS Public Access

Author manuscript

Neuroimage. Author manuscript; available in PMC 2017 January 15.

Published in final edited form as:

Neuroimage. 2016 January 15; 125: 74–83. doi:10.1016/j.neuroimage.2015.10.030.

Differential Aging of Cerebral White Matter in Middle-Aged and Older Adults: A Seven-Year Follow-up

Andrew R. Bender,
Center for Lifespan Psychology, Max Planck Institute for Human Development

Manuel C. Völkle, and
Department of Psychology, Humboldt University & Center for Lifespan Psychology, Max Planck Institute for Human Development

Naftali Raz
Institute of Gerontology & Department of Psychology, Wayne State University

Abstract

The few extant reports of longitudinal white matter (WM) changes in healthy aging, using diffusion tensor imaging (DTI), reveal substantial differences in change across brain regions and DTI indices. According to the last-in-first-out hypothesis of brain aging late-developing WM tracts may be particularly vulnerable to advanced age. To test this hypothesis we compared age-related changes in association, commissural and projection WM fiber regions using a skeletonized, region of interest DTI approach. Using linear mixed effects models, we evaluated the influences of age and vascular risk at baseline on seven-year changes in three indices of WM integrity and organization (axial diffusivity, AD, radial diffusivity, RD, and fractional anisotropy, FA) in healthy middle-aged and older adults (mean age = 65.4, SD = 9.0 years). Association fibers showed the most pronounced declines over time. Advanced age was associated with greater longitudinal changes in RD and FA, independent of fiber type. Furthermore, older age was associated with longitudinal RD increases in late-developing, but not early-developing projection fibers. These findings demonstrate the increased vulnerability of later developing WM regions and support the last-in-first-out hypothesis of brain aging.

Keywords

age; DTI; diffusivity; white matter; hypertension; longitudinal

Correspondence concerning this article should be addressed to Andrew R. Bender, Lentzeallee 94, 14195 Berlin, Germany. bender@mpib-berlin.mpg.de. Telephone: +49 30 82406–354.

Andrew R. Bender, Max Planck Institute for Human Development; Manuel Voelkle, Department of Psychology, Humboldt University & Max Planck Institute for Human Development; Naftali Raz, Institute of Gerontology & Department of Psychology, Wayne State University

The authors have no conflicts to declare.

1. Introduction

Healthy aging is associated with changes in brain structure and function. Although the evidence of differential age-associated regional brain shrinkage is consistent across multiple studies (see Raz & Rodrigue, 2006, Raz & Kennedy, 2009; Fjell et al. 2014 for reviews), considerably less is known about age-related changes in microstructural properties of cerebral white matter (WM). The invention of diffusion tensor imaging (DTI; Basser et al., 1994) enabled investigations of WM microstructure and organization through fitting brain water diffusion data to a tensor and quantifying diffusion properties in three principal directions by indices computed from the diffusion tensor eigenvalues: fractional anisotropy (FA), axial diffusivity (AD) and radial diffusivity (RD). In the past decade, numerous studies reported age-related differences in all DTI-derived indices (see Madden et al, 2012 for a review).

Cross-sectional studies in humans and postmortem examination of age-related WM differences in the brains of non-human primates suggest WM deterioration occurs in late adulthood (Peters, 2002). The pattern and magnitude of such age differences vary across brain regions and among DTI indices and are consistent with the notion of differential vulnerability (Hasan et al., 2009a; Hasan et al., 2009b; Kochunov et al., 2012; Lebel & Beaulieu, 2011; Lebel et al., 2012). The reasons for differential predilection of some WM regions to declines in aging remain unclear. Because the molecular composition of normal cerebral WM does not vary across the brain (Paus et al., 2014), it is unlikely that the observed pattern of WM age differences reflects differential sensitivity of cellular and molecular processes involved in WM maintenance.

Whereas cellular structure of WM is uniform throughout the brain, its local organization varies across the brain regions and tracts. Neuroanatomists identify three major classes of the cerebral WM: intracortical (incorporated in the layers of the gray matter), ‘‘superficial’’ (e.g., U-fibers) and long-range bundles of fibers or tracts (Paus et al., 2014). By considering the origins and targets of the long range tracts, WM fibers may be further classified into three major groups: projection, commissural, or association tracts (Catani, 2000). Significant heterochrony of WM development has been suggested by postmortem studies that report early emergence of the projection fibers and protracted maturation of the association tracts (Flechsig, 1901; Hermoye et al., 2006). Longitudinal DTI studies of infants and children are consistent with heterochronic development of the long-range WM tracts, although it remains unclear which processes (myelination, axon expansion or changes in cytoskeleton density) determine maturational WM changes observed on MRI (Simmonds et al., 2014; Giorgio et al., 2010; Paus, 2010; Lebel & Beaulieu, 2011; Bava et al., 2010).

Observations on differences and changes in WM across the lifespan prompted several hypotheses linking heterochronic age-related decrements in WM microstructure to common patterns of WM development. Specifically, the last-in-first-out hypothesis (Raz, 2000, 2001) postulates that tracts that are late to mature, and particularly late-myelinating fibers, are more vulnerable to insult and decline in later life (Gao et al., 2011; Lu et al., 2011). A stronger retrogenesis hypothesis posits a more specific mirroring of developmental progression by age-related course of decline (Reisberg et al., 1999; Brickman et al., 2012).

Testing of such hypotheses of WM aging is hampered by reliance on cross-sectional designs, which may inform about age-related differences, but are poorly suited for evaluating individual differences in change and may underestimate the rate of age-related longitudinal WM decline (Hofer & Sliwinski, 2001; Lindenberger et al. 2011). Longitudinal studies of other putative measures of brain health, such as regional volumes, have shown poor agreement with cross-sectional investigations (Raz et al., 2005; 2010; Pfefferbaum & Sullivan, 2015), but similar comparisons of WM measures are still scarce. To date, only a handful of studies have examined trajectories of WM change in healthy adults through application of DTI-derived indices of brain microstructure and organization (Barrick et al., 2010; Bender & Raz, 2015; Lövdén et al., 2014; Sullivan et al., 2010a; Sexton et al., 2014; Teipel et al., 2010). Notably, these studies were restricted to only two measurement occasions and hence could not elucidate the trajectories of WM aging. Only two studies to date have evaluated change over three or more occasions (Pfefferbaum et al., 2014; Vik et al., 2015). Moreover, these investigations (with exception of Bender & Raz, 2015 and Lövdén et al., 2014) did not attempt to examine individual differences in the rate of change, and did not take into account the influence of prevalent age-related risk factors (except Bender and Raz, 2015) and pathological WM changes (except Sexton et al., 2014; Bender and Raz, 2015).

The association between the burden of white matter hyperintensities (WMH) that are observed on T2-weighted MRI scans and reflect multiple age-related pathological processes (Erten-Lyons et al., 2013), and DTI indices of WM diffusion have been demonstrated in cross-sectional (Vernooij et al., 2008, 2009) and longitudinal (Sexton et al., 2014) studies. WMH reflect a diverse set of inter-related metabolic, inflammatory and vascular risk factors that affect the brain in ostensibly healthy adults (Jagust, 2013; Raz & Rodrigue, 2006; Kennedy & Raz, 2015). Elevated blood pressure and hypertension (even treated and reasonably well-controlled) are associated with differences in DTI-derived indices even in selective healthy samples (Artero et al., 2004; Bender & Raz, 2015; Burgmans et al., 2010; Kennedy & Raz, 2009; Raz, Rodrigue, Kennedy, & Acker, 2007; Raz et al., 2012). It is important, therefore, to include such factors in analyzing the trajectories of brain aging, especially in samples with significant proportion of older participants.

To address some of the outlined limitations of the extant studies, we sought to characterize the longitudinal changes in WM diffusion properties in a sample of healthy middle-aged and older adults, who were measured at one to four occasions over seven years. We hypothesized that the rate of change in diffusion properties of normal appearing WM over that period would differ by fiber tract type, and by the region. Specifically, in accordance with the last in-first-out hypothesis, we expected the greatest longitudinal decline in association fibers, lesser change in the commissural regions and relative stability of diffusion properties in the projection fibers. Furthermore, based on prior findings (Bender & Raz, 2015; Lövdén et al., 2014; Sexton et al., 2014), we hypothesized that advanced aging would be associated with greater declines in FA and increase in radial diffusivity (RD) compared to less pronounced changes in axial diffusivity (AD).

2. Methods

2.1 Participants

Participants were paid volunteers recruited from a major metropolitan area in the Midwestern United States by print media advertisements, flyers, and word of mouth. This sample overlaps with previously reported samples that were assessed at baseline (Kennedy & Raz, 2009) or on three occasions, with other brain indices (Raz et al., 2012). The sample analyzed here includes those who were at least 50 years of age at first DTI assessment, and had one to four longitudinal assessments.

At each measurement occasion, all participants provided written informed consent, in accord with the guidelines for human subject research established by the University Institutional Review Board and the Declaration of Helsinki. Participants were screened via self-report questionnaire for history of neurological and psychiatric disorders, cardiovascular disease other than physician diagnosed and medically treated essential hypertension, diagnosis or treatment for endocrine disorders, head injury accompanied by loss of consciousness for more than five min, use of anxiolytic, antidepressant, or antiepileptic medications, or consumption of more than three alcoholic beverages per day. In addition, participants were screened in the laboratory for cognitive impairment with the Mini Mental Status Examination (Folstein et al., 1975; baseline cutoff = 26), and for symptoms of depression with the Geriatric Depression Questionnaire (CES-D; Radloff, 1977; cut-off = 15). All participants reported right-hand dominance with scores > 75% on the Edinburgh Handedness Inventory (Oldfield, 1971).

The sample included 38 healthy adults (55% women), who were 50 to 84 years of age at first DTI assessment (mean age = 65.4, SD = 9.0 years). Men and women did not differ in age, MMSE scores, or blood pressure (Table 1). The mean education exceeded four years of college (mean education = 16.8, SD = 2.5 years), and there was only a nonsignificant trend for men to report more years of formal schooling compared to women. Furthermore, proportion of self-reported smoking, regular exercise or frequency thereof, and diagnosed hypertension did not differ as a function of participant sex. Eleven participants who developed additional health problems between the third and the fourth measurement occasions, did not differ from the remainder of the sample in baseline demographics, health characteristics, or rates of WM change (see Supplementary Materials 1.1 and Supplementary Table 1 for a complete description).

Although MRI scans were administered at four separate occasions (i.e., T1, T2, T3, and T4), because the DTI sequence was introduced to the protocol midway through the first wave (T1), the first 22 out of the 38 participants did not have DTI scans at T1. Thus, T2 occasion served as the baseline for those 22 participants. Across the sample, the mean intervals between consecutive occasions of measurement were: mean T1–T2 delay = 14.93 months (SD = 1.38; n = 13); mean T2–T3 delay = 15.58 months (SD = 2.65; n = 31); mean T3–T4 delay = 58.06 months (SD = 5.28; n = 19). In addition two participants underwent DTI scanning only at T2 and T4, and the mean delay for them was 81.00 months (SD = 5.65). Three participants had DTI scans only at T1 and T4, and the mean delay for this group was 86.00 months (SD = 0.08).

The sample included three participants who had only baseline measures - older adults (80.5, 73.3 and 67.5 years of age) who acquired contraindications to MRI (e.g., cardiac pacemaker) between the measurement occasions. By keeping them in the sample we gained a better understanding of the baseline cross-sectional relationship between the measures of interest and age. The remaining 35 participants completed at least one follow-up assessment: 13 participants completed two waves of assessment, 16 participants completed three measurement occasions, and six were scanned at all four occasions. As apparent from Figure 1, there is no relationship between participants' age and the length of participation in the study. The correlation between average age and number of measurement occasions is essentially zero ($r = 0.03$; $p = 0.83$). We therefore believe that potentially biasing influence of different numbers of measurement occasions on age-related changes is negligible.

At each measurement occasion, trained technicians measured participants' blood pressure. Assessments were taken while the participant was seated, from the left and right arms, on two separate days. Blood pressure measurements employed an auscultatory method to measure with diastole phase V for identification of diastolic pressure (Pickering et al., 2005). The values for both arms were averaged across days to obtain the mean systolic and diastolic pressure for each occasions reported in Table 1.

2.2 MRI acquisition

Across all occasions the participants were scanned on the same 1.5T Siemens Magnetom Sonata scanner (Siemens Medical. Systems, Erlangen, Germany). DTI data were acquired in the axial plane using a single-shot echo planar imaging (EPI) sequence with the following parameters: repetition time TR = 5400 ms, echo time TE = 97 ms; 6 gradient encoding directions with a b-value=1000 s/mm^2, one image with no diffusion weighting (b = 0), 10 averages; voxel size = 1.8 × 1.8 × 3.0 mm^3; distance factor = 0.

2.3 DTI Processing and Sampling

DTI processing employed a custom pipeline implemented in a Bourne shell using the FMRIB software library (FSL; Jenkinson et al., 2012) v5.0.2 (Analysis Group, FMRIB, Oxford, UK). See Bender and Raz (2015) for a complete description of all pipeline functions. The pipeline was designed to maintain the original signal characteristics from multiple measurement occasions by sampling from native space data, in an effort to minimize undue potential interpolation and artifacts due to spatial normalization and transformations. In addition, we restricted data to exclude WMH and cerebrospinal fluid (CSF) from analysis. We used the tract-based spatial statistics (TBSS; Smith, 2006) pipeline only to create a common, group-wise skeleton mask and to deproject this skeletonized WM mask and skeletonized probabilistic atlas-based regions of interest (ROIs) for native space sampling.

2.3.1 Intra-subject Longitudinal Common Space Registration—The present processing approach used the TBSS pipeline to 1) generate a group-wise WM skeleton, and then to 2) deproject atlas-derived ROIs restricted to the WM skeleton for sampling DTI indices from individual native space. However, to optimize within-person spatial correspondence between measurement occasions prior to group-wise normalization and

skeletonization with TBSS pipeline, we co-registered the individual b0 images for each participant in order to calculate a common, intermediate space between occasions (Figure 2a). This method accounted for the variable number of data points per participant and individual differences in timing of measurement (i.e., participants measured on first and third occasions, vs. participants measured on second, third, and fourth occasions). For participants with four longitudinal data points, the Time 2 (T2) b0 image was registered to Time 1 (T1) image, and Time 4 (T4) image was registered to the one obtained at Time 3 (T3). The transformation matrices from each registration were used to calculate the intermediate space between the images. Subsequently, the co-registration of two intermediate space images was similarly used to determine a final space common across all measurement occasions. If only three measurements were available, the T2 image was registered to the one obtained at T1 and the T3 image was then registered with the intermediate T1–T2 space.

2.3.2 WMH/CSF Masking—The pipeline used the FAST tool (Zhang et al., 2001) to segment the native b0 images into six separate masks based on voxel intensity (Figure 2b). The segmented masks for the T2-weighted b0 images included peripheral image noise outside the brain, cortical ribbon and CSF-cortex interface, hyperintense ventricular regions reflecting CSF or WMH, as well as normal appearing WM, WM-cortex interface and subcortical gray matter nuclei. The two segmented masks representing normal appearing WM were summed and binarized into a WM mask that excluded CSF and WMH for each participant. The resulting WM mask for each participant was inspected in comparison with the native b0 image to ensure the accuracy of the segmentation.

2.3.3 Tensor Fitting & WM Skeleton Mask Creation—We employed the default FSL tensor fitting procedures on native space images, while also saving the tensor data. Following calculation of the common image space (see 2.3.1, above), the b-vectors were rotated accordingly, and the saved tensor components were refitted into the common space for each subject. Next, we submitted the resultant, common space FA images to the TBSS pipeline, which nonlinearly registered the FA images to standard MNI space and derived a group-wise WM skeleton one voxel in width. The final TBSS processing step used a threshold of 0.3 to limit the more peripheral and less reliable aspects of the WM skeleton.

2.3.4 WM Skeleton Deprojection & Atlas-based ROI Creation—Following TBSS skeletonization, the pipeline used the native tbss_deproject routine to diffeomorphically deproject 1) the mean group skeleton mask, and 2) skeletonized, WM atlases to subjects' individual native space (Figure 2c). The JHU-ICBM white matter atlas labels at 1mm, and the JHU-ICBM white matter tractography atlas were transformed to native space using the inverse transformation matrices from TBSS processing and common space determination. This approach limited atlas deprojection only to the mean WM skeleton. Following atlas deprojection along the WM skeleton, separate skeletonized ROIs were generated. These were used to sample FA, AD, and RD from the native space DTI data, masked to exclude CSF/WMH. In addition, the masks for genu and splenium were used subtractively with those for forceps minor and major, respectively, so that these regions might be sampled separately.

2.3.4 ROIs—To limit the likelihood of spurious findings, we chose 12 ROIs for analysis, based on the extant findings relating age to DTI-based WM measures. The selected ROI set was comprised of seven inherently bilateral ROIs - five association fiber tracts (cingulum bundle [CB], inferior frontal-occipital fasciculus [IFOF], inferior longitudinal fasciculus [ILF], superior longitudinal fasciculus [SLF], uncinate fasciculus [UF]), and two projection (anterior limb of internal capsule [ALIC], posterior limb of internal capsule [PLIC]), as well as five commissural ROIs including three sampled from the midline (corpus callosum [CC] genu, body, and splenium) and two sampled bilaterally (forceps minor and forceps major). The latter provided more distal values for anterior and posterior commissural fiber tracts.

2.4 Statistical analyses

Linear mixed effects (LME) models were used to account for the hierarchical structure of the $j = 1, \ldots, (J = 12)$ ROIs nested within individuals $i = 1, \ldots, (N = 38)$, and measured across a total of $t = 1, \ldots, (T = 4)$ time points. Sex was included as a covariate in all models and if found non-significant, removed from further analyses. Three separate analyses were carried out for fractional anisotropy (FA), radial diffusivity (RD), and axial diffusivity (AD). For each DTI index, average values across hemispheres were computed for all bilateral ROIs. Analyses were carried out using the lme4 (Bates et al., 2014) and lmerTest (Kuznetsova et al., 2014) packages in R (R Core Team, 2014). The full model is given in Equation 1:

$$\begin{aligned} y_{ijt} = {} & \beta_0 + \beta_1\, Time_{it} + \beta_2\, Initial\ Age_{it_o} \\ & + \beta_3\, Projection_j + \beta_4\, Commissural_j \\ & + \beta_5\, HBP_i \\ & + \beta_6\, Time_{it} \times Initial\ Age_{it_o} + \beta_7\, Time_{it} \times Projection_j + \beta_8\, Time_{it} \\ & \times Commissural_j \\ & + \zeta_i + \zeta_j + \varepsilon_{ijt}. \end{aligned}$$

The dependent variable y_{ijt} denotes one of the three DTI indices for individual *i*, ROI *j* and time point *t*. To reduce multicollinearity and to ease parameter interpretation, participants' age at the first measurement occasion ($Initial\ Age_{it_0}$) was group-mean centered by subtracting the average age at that time point (65.40 years). Likewise, participants' age at each measurement occasion ($Time_{it}$) was centered at 70, which is close to the overall median of age (68.17 years). Fiber type (association, projection, commissural) and a binary (yes, no) high blood pressure diagnosis (HBP_i) were entered as dummy variables, with association fibers and normal blood pressure serving as baseline measures for comparison. Thus, the intercept β_0 reflects the overall level of FA, RD, AD, respectively, in association fibers for a 70-year old person with normal blood pressure, who entered the study at an age of 65.40 years. Higher order interactions were tested for alterations in the magnitude of change associated with differences in baseline age ($Time_{it} \times Initial\ Age_{it_0}$) , or by fiber type ($Time_{it} \times projection_j \times Time_{it} \times commissural_j$). Var($\zeta_i$), Var($\zeta_j$), Var($\varepsilon_{ijt}$) denote the variance components for persons, ROIs, respectively, as well as the remaining error variance.

Out of a maximal number of 1824 observations = [38 participants × 4 occasions × 12 regions], 1212 could be realized. Parameter estimation in the presence of missingness was

carried out under the missing at random assumption by means of restricted maximum likelihood estimation. *P*-values of parameter estimates are calculated based on Satterthwaite's approximation as implemented in lmerTest (Kuznetsova et al., 2014), whereas variance components were tested based on likelihood ratio comparisons using unrestricted maximum likelihood estimation. To limit potentially spurious findings, we used an alpha value that accounted for the comparison of effects across the three different DTI indices, we adjusted the criterion for significance to $\alpha = 0.0167$, for tests of effects and interactions across the three DTI indices for both the initial and the follow-up models.

3. Results

3.1 LME Analyses for AD, RD, and FA

All three LME analyses summarized in Table 2 revealed significant random effects of ID and ROI (for all, $p < .001$). The fixed effects in the LME model for AD showed that AD declined over time across all examined fiber types, with the steepest change in association fibers. In addition, older age at baseline was associated with higher AD across ROIs, but was unrelated to the rate of decline. Participants reporting diagnosed and treated hypertension at baseline had higher AD across the regions and fiber types ($p = .020$), but this difference was rendered non-significant by Bonferroni correction.

The model for RD showed that older age at baseline was associated with higher baseline values and greater longitudinal increases of RD. The RD increases were significant in association and commissural fibers, whereas projection fibers displayed a small but significant decrease in RD. The association between hypertension diagnosis and higher baseline RD ($p = .050$) was not significant after Bonferroni correction.

The FA model analyses revealed FA decline in all three fiber types, with steeper decline in association regions relative to the projection and commissural fibers. Older participants showed greater drop in FA, although higher baseline age was unrelated to FA values.

3.2 Follow-Up LME Analyses

We used the same LME approach to conduct follow-up analyses, aimed at testing two specific hypotheses. Recent findings from a two-occasion, longitudinal DTI study (Bender & Raz, 2015) that used a similar DTI pipeline for examined WM changes in an adult lifespan sample showed linear AD reductions in both ALIC and PLIC, but FA increases in PLIC over time. Because those findings suggest that WM development may continue in early maturing motor tracts, we sought to test for such effects in this sample of middle-aged and older adults. To test this hypothesis, we compared the two projection fiber regions ALIC and PLIC to assess differential change, association with age, and the interaction thereof. Post hoc models for AD in projection fibers revealed change over time, and showed that older age at baseline was associated with higher AD. AD in PLIC declined over time as it did in the association and commissural fibers, despite a lack of change in ALIC.

3.2.1 Follow-Up LME Analyses - Projection Fibers—The follow-up analysis of RD in projection fibers showed a positive association with age at baseline. Although there was no significant mean change in ALIC, older age was associated with stronger increases in RD

over time. In comparison with ALIC, RD in PLIC also showed linear reductions over time (p = .046), but this was not significant following Bonferroni correction. In addition, post hoc models of FA for projection fibers revealed a significant time × age interaction suggesting that older age was associated with greater FA decline in ALIC, and a significant time × association fiber interaction reflecting steeper linear declines in those fibers, relative to ALIC.

3.2.2 Follow-Up LME Analyses – Commissural Fibers—Bender and Raz (2015) reported FA increases and RD decreases in CC body, in contrast to opposite effects in the remaining commissural regions. To test for such effects in the present sample, we examined the age differences, change over time and the bivariate interaction between change and baseline age for CC body, in comparison with the other commissural ROIs. Older age was associated with higher AD at baseline, and AD in remaining commissural fibers showed significant declines. A significant negative time × association fiber ROI interactions showed greater decline of AD in association compared to commissural fibers (splenium and genu and forceps minor, major). In contrast, nonsignificant positive trends toward both a time × CC body interaction (p = .036) and time × projection fiber interaction (p = .053) suggested marginal attenuations in linear decline over time in CC body AD relative to other commissural fiber ROIs. Furthermore, the post hoc models examined whether hypertension was associated with differential change. The AD model revealed no significant higher order interaction of time × CC body × hypertension (p = .628).

The follow-up analysis of RD in commissural fibers showed that at baseline, older age and diagnosed hypertension were associated with higher RD, although the latter did not survive Bonferroni correction (p = .047). Older age at baseline was associated with greater longitudinal increases in commissural RD. Relative to remaining commissural fibers, RD in projection regions showed marginally attenuated linear increases over time, while time exacerbated increases RD in association fiber regions, although these effects were no longer significant following Bonferroni correction (for both, p = .033).

Post hoc models of FA in commissural ROIs showed significant decline in FA over time in anterior and posterior commissural fibers. There were no differences between CC body and the other commissural fiber ROIs in values or rate of change in DTI-derived indices. A significant time × age interaction reflected steeper FA declines in older participants. A significant negative time × association fiber region interactions showed greater longitudinal FA decline in association fibers compared to the remaining commissural fibers. In contrast, a positive time × projection fiber interaction indicated attenuated linear decline over time in FA for projection compared to remaining commissural fibers.

4. Discussion

The central finding of this study is the differential vulnerability of association pathways to aging. Diffusion properties in association WM tracts deteriorated more than in the commissural and projection fibers, and in some of them the pace of decline accelerated with age. Notably, these results are based on a seven-year follow-up with up to four measurement occasions.

Differential AD reduction in association fibers replicates our previous finding (Bender & Raz, 2015), but contradicts other studies that reported increase in AD between the baseline and a single follow-up (Barrick et al., 2010; Sexton et al., 2014). The reason for this discrepancy is unclear and possible sources of disagreement include differences in populations on which the studies were conducted, or different analytical methods, i.e., the use of DTI difference maps and voxel-wise *t*-tests (Barrick et al., 2010; Sexton et al., 2014) versus latent and mixed effects models of mean values by ROI (Bender & Raz, 2015). In agreement with the abovementioned studies, we observed no age-related acceleration of AD change.

Significant increases in RD reported here are in accord with some of the previous reports (Barrick et al., 2010; Sexton et al., 2014; but see Bender & Raz, 2015). Furthermore, older age was linked to steeper increase in RD over time. Whereas the greatest linear increases in RD were noted in the association fiber regions, the smallest change was observed in projection fibers. Thus, the present findings demonstrate heightened vulnerability of association regions to aging.

In line with the previous reports FA showed decline in all three fiber groups (Barrick et al., 2010; Teipel et al., 2010; Sexton et al., 2014; Bender & Raz, 2015), but decline in association regions was steeper in comparison to the projection and commissural fibers. Age-related acceleration of change was observed in FA and RD (contrary to Barrick et al, 2010; Sexton et al., 2014; Bender & Raz, 2015) but not AD (in accord with Barrick et al., 2010; Sexton et al., 2014 but in contradiction to Bender & Raz, 2015). It is worth noting, however, that with two exceptions (Pfefferbaum et al., 2014; Vik et al., 2015) all previous longitudinal studies have been conducted over only two occasions and thus, unlike the current study, were not suited for examination of the trajectory of change. Pfefferbaum and colleagues (2014) used TBSS to compare aging trajectories in healthy adults and persons with history of alcohol dependence and showed widespread age-related declines in both groups. The other prior longitudinal study that evaluated change over two to three measurement occasions (Vik et al., 2015), restricted WM evaluation to FA in subcortical-cortical fiber tracts, and only used paired-sample t-tests to evaluate change over time. Furthermore, if WM declines with age, then inclusion of samples with greater age ranges may also bias the findings against showing mean declines.

Understanding DTI findings and interpreting DTI indices as proxies for WM microstructural characteristics is a challenging task. The three DTI indices reported here are believed to reflect multiple tissue properties (Beaulieu, 2002, 2012; Jones et al., 2013). For example, reduced RD has been linked to myelin breakdown and altered membrane permeability, whereas AD reduction is taken to reflect damage to many aspects of axonal structure (Song et al., 2002, 2003, 2005; Sun et al., 2006, 2008). A combination of increased RD and reduced AD, as observed here, may be indicative of Wallerian degeneration (Ford & Hackney, 1997; Ford et al., 1998; Pierpaoli et al., 2001; Sun et al., 2008), a slow-paced process whose molecular underpinnings remain unclear (Vargas & Barres, 2007). The most global index of white matter organization, FA, combines information from all components of the diffusion tensor, and is largely dependent on fiber packing density and tortuosity, axonal membrane thickness and permeability, intercellular space size as well as myelin

content and integrity (Beaulieu, 2002). In light of these possibilities, the findings reported here may be taken to reflect as deterioration of axonal architecture, including damage to the neurofilaments and microtubular transport system, loss of myelin membrane integrity, reduction in fiber density, increase in extracellular space and loss of organization in white matter tracts (Coleman, 2005; Vargas & Barres, 2007; Paus et al., 2014). All these phenomena are likely to lead to age-related decline in the quality of information transmission between cortical regions that the WM fibers connect. It is plausible that the long association tracts that connect cortical region known for their vulnerability to aging (e.g., prefrontal and inferior parietal, e.g., Raz et al., 2005) are in a particularly high risk for age-related decline because of their targets and their developmental history.

Differential vulnerability of the association fibers conforms to the hypothesized first-in-last-out order of regional brain aging (Raz, 2000; 2001). The least affected regions (e.g., PLIC) are early-to-mature tracts that myelinate at term (Dubois et al., 2014) and in premature infants are the first to catch up with those of their counter parts who were delivered at term (Kersbergen et al., 2014). In contrast to PLIC, fibers in ALIC develop considerably later, are marked by greater organizational heterogeneity, and appear more vulnerable to the effects of age (Axer & Keyserlingk, 2000; Makris et al., 2007; Sullivan et al., 2010a). Commissural fibers, that showed moderate change over time in this sample, mature later than the projection tracts but catch up with at the early stages of postnatal development (Sadeghi et al, 2013). In contrast, association fibers whose myelination starts after birth and continues into adulthood (Dubois et al., 2014) showed the most pronounced decline over the seven-year period.

A life-long process of myelin synthesis and maintenance is balanced by continuous loss (see Bartzokis, 2004 for review). As older individuals experience difficulties in myelin maintenance and repair (Ibanez et al., 2003) this equilibrium gradually shifts, myelin sheath deteriorates and myelinated fibers are disproportionally lost at least in some key regions of the central nervous system (Peters, 2002; Sandell & Peters, 2003). Thus, loss of myelin may account for some of the observed changes, particularly, increase in RD. Moreover, the temporal pattern of myelination (Flechsig, 1901) appears to correspond, in reverse, to the observed pattern of age-related declines.

Myelin, however, cannot be the whole story of WM aging as reflected in DTI indices, because its diffusion properties are determined by multiple components in addition to myelin, including axonal membranes, axonal cytoskeleton and the system of microtubules that runs along the axon, as well as the density and diameter of the axons (Coleman, 2005; Paus et al., 2014). Whereas myelin sheath is affected by aging (Peters, 2002; Bartzokis, 2004), neuropathology studies point to reduction in axonal density and increase in axon caliber as important contributors to age-related WM degeneration (Hou & Pakkenberg, 2012). Changes in FA observed in this and other studies may result from alterations in any or all of these factors. Thus, different DTI-derived indices exhibit differential sensitivity to detecting change over time and follow different trajectories. There appears to be a good agreement across studies with regards to the downward trend in FA, but lesser consistency in age trajectories of the other diffusivity measures.

As noted in the studies of other brain properties, such as regional volume (Raz et al., 2005; 2010; Pfefferbaum & Sullivan, 2015) or iron content (Daugherty et al., 2015), changes inferred from cross-sectional age differences in DTI indices do not correspond well to the observed longitudinal patterns of change (Bender & Raz, 2015). At baseline, age was associated with higher AD, suggesting the direction of change that was the opposite of the one observed in longitudinal follow-ups. Unlike FA and RD, older age was not associated with increased AD change. Longitudinal AD reductions in middle-aged and older adults may reflect alterations in axonal diameter, density, or in the prevalence of crossing fibers (Beaulieu, 2012; Jones et al., 2013; Jones & Cercignani, 2010) and it is unclear which of these processes flag neurodegenrative processes and which are signs of ongoing normal re-organization. With respect to RD, cross-sectional and longitudinal findings agreed as higher RD at baseline was associated with older age and showed increase over time. Finally, baseline age was unrelated to FA values, yet older participants showed steeper decline in FA. It is possible that middle-aged and older adults selected for optimal health evidenced attenuated age differences at baseline, yet still exhibited age-related decline.

In contrast to recently published findings in a sample of healthy persons covering the adult lifespan (Bender & Raz, 2015), we did not observe significant individual differences in change. The lack of significant individual variability in trajectories of change may reflect a relative homogeneity of this sample composed of middle-aged and older adults who were optimally healthy at baseline. The lack of individual differences in DTI indices is in line with the lack of individual variability in WMH trajectories observed in the first three waves of this sample (Raz et al., 2012).

4.1 Vascular Risk and Aging of Cerebral White Matter

In the previous study on an independent sample drawn from the same population (Bender & Raz, 2015), we noted a modulating role of composite metabolic risk factor (of which hypertension is a part) on WM changes. However, that study revealed a selection bias: in younger adults but not in older participants who were screened for optimal health, greater WM decline was associated with elevated risk for metabolic syndrome. Here, a single available vascular risk indicator (hypertension diagnosis) showed only weak associations with WM variability and the results did not survive the correction for multiple comparisons. Bonferroni correction may be overly conservative and in deciding whether to apply it, one needs to balance the risk of spurious findings versus the focus on selected hypotheses based on prior findings (Bender & Raz, 2015; Lövdén et al., 2014). Thus, the impact of vascular risk on age-related decline in WM microstructure of persons who are free of age-related diseases remains unclear.

4.2 Limitations and Future Directions

Although the present study represents an important initial step in characterizing longitudinal WM changes in healthy aging, its small sample size places limits on a meaningful investigation of potential additional influences, such as genetic risk for dementia, and vascular disease. In the present study, we sampled mean values from skeletonized WM regions defined according to probabilistic atlases. Although comparison of correlations between age and change in each the three DTI indices may provide some insight into

differential patterns of age-associated change across studied brain regions, such analyses are hampered by the study's relatively modest sample size and limited statistical power that preclude including all indices and regions in a single model. Thus, future longitudinal studies with larger samples should be encouraged to compare age-related changes across DTI parameters. Tractography may provide a more precise anatomical demarcation and yield more precise assessment of the WM in these tracts. Furthermore, tractography methods designed to evaluate specific areas affected within a given WM tract may help better understand whether age and VR yield more localized effects on age-related WM decline (Colby et al., 2012; Davis et al., 2009).

The present findings showed differences in rates of decline between mean values sampled from regions reflecting different WM fiber types. Limiting the DTI data to six gradient directions with 10 averages may have improved the limited signal-to-noise on 1.5T field strength, but precluded performing fiber tracking. Thus, we were unable to test more specific hypotheses related to retrogenesis, or testing for graded posterior to anterior reductions FA (Davis et al., 2009) or superior-inferior gradients in projection fibers (Sullivan et al., 2010b; Zahr, Rohlfing, Pfefferbaum, & Sullivan, 2009). Nonetheless, as prior evidence for greater vulnerability of later-developing WM regions has been limited to cross-sectional data, the present longitudinal findings provide an important basis in establishing the last-in-first-out hypothesis.

In addition, our method for excluding CSF and WMH was based solely on segmentation of the b0 image. The traditional reference for both qualitative and volumetric WMH evaluation has been FLAIR images that are frequently of higher spatial resolution and attenuate the signal of CSF to assist the division of periventricular WMH. Although we used this in combination with WM skelektonization, it is possible that some limited voxels contained signal from lesioned WM. However, the sampled DTI values represent mean signal from all voxels in the ROI, which may mitigate such concerns.

The image processing approach employed in the present study combined elements of prior, two-occasion DTI studies (Bender & Raz, 2015; Engvig et al., 2011) for intra-subject registration, prior to estimation of the WM skeleton using TBSS. This processing approach sampled from skeletonized atlas-based ROIs, deprojected to native space, but has not been empirically compared against other, recent developments for longitudinal WM registration and sampling (Keihaninejad et al., 2013). Although visual inspection showed it to be effective, our method for excluding WMH and CSF is less sophisticated in comparison to methods leveraging data from multiple image types in classifying and segmenting WMH. The combination of sampling from skeletonized WM data, masked to exclude CSF, WMH, and noisy voxels may minimize any undue influence of those sources of signal variability on mean DTI parameters.

Reliance on a popular but coarse single-tensor approach implemented in DTI is another methodological limitation. As recently argued in a cogent review of its limitations, DTI yields only very crude indices of WM microstructural integrity and organization (Jones et al., 2013; Jones & Cercignani, 2010) and cannot distinguish the effects of myelin, axonal

diameter, axonal density, fiber orientation and extracellular space configuration on water diffusion in WM.

Although axons occupy about 87% of the space taken by the WM, the vast majority of axons are located within intracortical and superficial compartments and only 4% of them belong to the long-range fiber tracts (Wang et al., 2008, see Paus et al, 2014 for review). Thus, methods employed in this study could examine only a small proportion of the WM constitutents. Although all participants were scanned on the same MRI scanner on all occasions of measurement, there is some possibility that routine software upgrades could modify change trajectories (Takao et al., 2012). However, data collection in this study began before the use of MR phantoms to control for effects of scanner drift and software upgrades. Thus, the use of phantoms as a control against such potential confounds should be strongly encouraged in future longitudinal diffusion imaging studies of aging and adult development.

4.3 Conclusions

From middle age onward aging is associated with steeper RD and FA change in association fibers than in commissural or projection regions. Within the latter, diffusion characteristics of the earlier-developing posterior limb were better maintained across the examined period than those of the later-developing anterior limb of the internal capsule. These findings yield support to the last-in-first-out hypothesis of brain aging.

Supplementary Material

Refer to Web version on PubMed Central for supplementary material.

Acknowledgments

This work was supported in part by grants from the National Institute on Aging grants R03- AG024630 and R37-AG-011230 to NR.

References

Artero S, Tiemeier H, Prins ND, Sabatier R, Breteler MM, Ritchie K. Neuroanatomical localisation and clinical correlates of white matter lesions in the elderly. Journal of neurology, neurosurgery, and psychiatry. 2004; 75:1304–1308.10.1136/jnnp.2003.023713

Barrick TR, Charlton RA, Clark CA, Markus HS. White matter structural decline in normal ageing: A prospective longitudinal study using tract-based spatial statistics. Neuroimage. 2010; 51:565–577.10.1016/j.neuroimage.2010.02.033 [PubMed: 20178850]

Bartzokis G, Sultzer D, Lu PH, Nuechterlein KH, Mintz J, Cummings JL. Heterogeneous age-related breakdown of white matter structural integrity: Implications for cortical "disconnection" in aging and Alzheimer's disease. Neurobiol Aging. 2004; 25:843–851.10.1016/j.neurobiolaging.2003.09.005 [PubMed: 15212838]

Basser PJ, Mattiello J, LeBihan D. Estimation of the effective self-diffusion tensor from the NMR spin echo. J Magn Reson B. 1994; 103:247–254. [PubMed: 8019776]

Bates, D.; Maechler, M.; Bolker, B.; Walker, S. Lme4: Linear mixed-effects models using eigen and s4. R package version 1.1–7. 2014. This is computer program (R package). The URL of the package is: http://CRAN.R-project.org/package=lme4

Bava S, Thayer R, Jacobus J, Ward M, Jernigan TL, Tapert SF. Longitudinal characterization of white matter maturation during adolescence. Brain Res. 2010; 1327:38–46.10.1016/j.brainres.2010.02.066 [PubMed: 20206151]

Beaulieu C. The basis of anisotropic water diffusion in the nervous system - a technical review. NMR Biomed. 2002; 15:435–455.10.1002/nbm.782 [PubMed: 12489094]

Beaulieu, C. The biological basis of diffusion anisotropy. In: Johansen-Berg, H.; Behrens, TE., editors. Diffusion MRI: From quantitative measurement to *in vivo* neuroanatomy. Academic Press; 2012. p. 106-126.

Bender AR, Raz N. Normal-appearing cerebral white matter in healthy adults: Mean change over two years and individual differences in change. Neurobiol Aging. 2015; 36:1834–1848.10.1016/j.neurobiolaging.2015.02.001 [PubMed: 25771392]

Brickman AM, Meier IB, Korgaonkar MS, Provenzano FA, Grieve SM, Siedlecki KL, Wasserman BT, Williams LM, Zimmerman ME. Testing the white matter retrogenesis hypothesis of cognitive aging. Neurobiol Aging. 201110.1016/j.neurobiolaging.2011.06.001

Burgmans S, van Boxtel MP, Gronenschild EH, Vuurman EF, Hofman P, Uylings HB, Jolles J, Raz N. Multiple indicators of age-related differences in cerebral white matter and the modifying effects of hypertension. Neuroimage. 2010; 49:2083–2093.10.1016/j.neuroimage.2009.10.035 [PubMed: 19850136]

Catani M. Diffusion tensor magnetic resonance imaging tractography in cognitive disorders. Curr Opin Neurol. 2006; 19:599–606.10.1097/01.wco.0000247610.44106.3f [PubMed: 17102700]

Colby JB, Soderberg L, Lebel C, Dinov ID, Thompson PM, Sowell ER. Along-tract statistics allow for enhanced tractography analysis. Neuroimage. 2012; 59:3227–3242.10.1016/j.neuroimage.2011.11.004 [PubMed: 22094644]

Coleman M. Axon degeneration mechanisms: Commonality amid diversity. Nature Reviews Neuroscience. 2005; 6:889–898. [PubMed: 16224497]

Daugherty AM, Haacke EM, Raz N. Striatal iron content predicts its shrinkage and changes in verbal working memory after two years in healthy adults. The Journal of Neuroscience. 2015; 35:6731–6743. [PubMed: 25926451]

Davis SW, Dennis NA, Buchler NG, White LE, Madden DJ, Cabeza R. Assessing the effects of age on long white matter tracts using diffusion tensor tractography. Neuroimage. 2009; 46:530–541.10.1016/j.neuroimage.2009.01.068 [PubMed: 19385018]

Dubois J, Dehaene-Lambertz G, Kulikova S, Poupon C, Huppi PS, Hertz-Pannier L. The early development of brain white matter: A review of imaging studies in fetuses, newborns and infants. Neuroscience. 2014; 276:48–71.10.1016/j.neuroscience.2013.12.044 [PubMed: 24378955]

Erten-Lyons D, Woltjer R, Kaye J, Mattek N, Dodge HH, Green S, Tran H, Howieson DB, Wild K, Silbert LC. Neuropathologic basis of white matter hyperintensity accumulation with advanced age. Neurology. 2013; 81:977–983. [PubMed: 23935177]

Fjell AM, McEvoy L, Holland D, Dale AM, Walhovd KB. Alzheimer's Disease Neuroimaging, I. What is normal in normal aging? Effects of aging, amyloid and Alzheimer’s disease on the cerebral cortex and the hippocampus. Prog Neurobiol. 2014; 117:20–40.10.1016/j.pneurobio.2014.02.004 [PubMed: 24548606]

Flechsig P. Developmental (myelogenic) localisation of the cerebral cortex in the human subject. Lancet. 1901; 158:1027–1030.

Folstein MF, Folstein SE, McHugh PR. "Mini-mental state". A practical method for grading the cognitive state of patients for the clinician. J Psychiatr Res. 1975; 12:189–198. [PubMed: 1202204]

Ford JC, Hackney DB. Numerical model for calculation of apparent diffusion coefficients (ADC) in permeable cylinders—comparison with measured ADC in spinal cord white matter. Magn Reson Med. 1997; 37:387–394. [PubMed: 9055229]

Ford JC, Hackney DB, Lavi E, Phillips M, Patel U. Dependence of apparent diffusion coefficients on axonal spacing, membrane permeability, and diffusion time in spinal cord white matter. J Magn Reson Imaging. 1998; 8:775–782. [PubMed: 9702877]

Gao J, Cheung RT, Lee TM, Chu LW, Chan YS, Mak HK, Zhang JX, Qiu D, Fung G, Cheung C. Possible retrogenesis observed with fiber tracking: An anteroposterior pattern of white matter disintegrity in normal aging and Alzheimer’s disease. Journal of Alzheimer's disease : JAD. 201110.3233/JAD-2011-101788

Giorgio A, Watkins KE, Chadwick M, James S, Winmill L, Douaud G, De Stefano N, Matthews PM, Smith SM, Johansen-Berg H, James AC. Longitudinal changes in grey and white matter during adolescence. Neuroimage. 2010; 49:94–103.10.1016/j.neuroimage.2009.08.003 [PubMed: 19679191]

Hasan KM, Iftikhar A, Kamali A, Kramer LA, Ashtari M, Cirino PT, Papanicolaou AC, Fletcher JM, Ewing-Cobbs L. Development and aging of the healthy human brain uncinate fasciculus across the lifespan using diffusion tensor tractography. Brain Res. 2009; 1276:67–76.10.1016/j.brainres.2009.04.025 [PubMed: 19393229]

Hasan KM, Kamali A, Iftikhar A, Kramer L, Papanicolaou A, Fletcher J, Ewingcobbs L. Diffusion tensor tractography quantification of the human corpus callosum fiber pathways across the lifespan. Brain Res. 2009; 1249:91–100.10.1016/j.brainres.2008.10.026 [PubMed: 18996095]

Hermoye L, Saint-Martin C, Cosnard G, Lee SK, Kim J, Nassogne MC, Menten R, Clapuyt P, Donohue PK, Hua K, Wakana S, Jiang H, van Zijl PC, Mori S. Pediatric diffusion tensor imaging: Normal database and observation of the white matter maturation in early childhood. Neuroimage. 2006; 29:493–504.10.1016/j.neuroimage.2005.08.017 [PubMed: 16194615]

Hofer S, Sliwinski MJ. Understanding ageing: An evaluation of research designs for assessing the interdependence of ageing-related changes. Gerontology. 2001; 47:341–352. [PubMed: 11721149]

Hou J, Pakkenberg B. Age-related degeneration of corpus callosum in the 90+ years measured with stereology. Neurobiol Aging. 2011

Ibanez C, Shields S, El-Etr M, Leonelli E, Magnaghi V, Li W-W, Sim F, Baulieu E-E, Melcangi R, Schumacher M. Steroids and the reversal of age-associated changes in myelination and remyelination. Prog Neurobiol. 2003; 71:49–56. [PubMed: 14611867]

Jagust W. Vulnerable neural systems and the borderland of brain aging and neurodegeneration. Neuron. 2013; 77:219–234.10.1016/j.neuron.2013.01.002 [PubMed: 23352159]

Jenkinson M, Beckmann CF, Behrens TE, Woolrich MW, Smith SM. FSL. Neuroimage. 2012; 62:782–790.10.1016/j.neuroimage.2011.09.015 [PubMed: 21979382]

Jones DK, Cercignani M. Twenty-five pitfalls in the analysis of diffusion MRI data. NMR Biomed. 2010; 23:803–820.10.1002/nbm.1543 [PubMed: 20886566]

Jones DK, Knosche TR, Turner R. White matter integrity, fiber count, and other fallacies: The do's and don'ts of diffusion MRI. Neuroimage. 2013; 73:239–254.10.1016/j.neuroimage.2012.06.081 [PubMed: 22846632]

Kennedy KM, Raz N. Pattern of normal age-related regional differences in white matter microstructure is modified by vascular risk. Brain Res. 2009; 1297:41–56. [PubMed: 19712671]

Kennedy, KM.; Raz, N. Normal aging of the brain. In: Toga, AW., editor. Brain mapping. Academic Press; Waltham: 2015. p. 603-617.

Kersbergen KJ, Leemans A, Groenendaal F, van der Aa NE, Viergever MA, de Vries LS, Benders MJ. Microstructural brain development between 30 and 40 weeks corrected age in a longitudinal cohort of extremely preterm infants. Neuroimage. 2014; 103:214–224. [PubMed: 25261000]

Kochunov P, Williamson DE, Lancaster J, Fox P, Cornell J, Blangero J, Glahn DC. Fractional anisotropy of water diffusion in cerebral white matter across the lifespan. Neurobiol Aging. 2012; 33:9–20. [PubMed: 20122755]

Kuznetsova, A.; Brockhoff, PB.; Christensen, RHB. R package version 2. 2013. Lmertest: Tests for random and fixed effects for linear mixed effect models (lmer objects of lme4 package).

Lebel C, Beaulieu C. Longitudinal development of human brain wiring continues from childhood into adulthood. The Journal of neuroscience : the official journal of the Society for Neuroscience. 2011; 31:10937–10947.10.1523/JNEUROSCI.5302-10.2011 [PubMed: 21795544]

Lebel C, Gee M, Camicioli R, Wieler M, Martin W, Beaulieu C. Diffusion tensor imaging of white matter tract evolution over the lifespan. Neuroimage. 2012; 60:340–352.10.1016/j.neuroimage.2011.11.094 [PubMed: 22178809]

Lindenberger U, von Oertzen T, Ghisletta P, Hertzog C. Cross-sectional age variance extraction: What's change got to do with it? Psychol. Aging. 2011; 26:34–47.10.1037/a0020525

Lövdén M, Kohncke Y, Laukka EJ, Kalpouzos G, Salami A, Li TQ, Fratiglioni L, Backman L. Changes in perceptual speed and white matter microstructure in the corticospinal tract are

associated in very old age. Neuroimage. 2014; 102(Pt 2):520–530.10.1016/j.neuroimage.2014.08.020 [PubMed: 25139001]

Lu PH, Lee GJ, Raven EP, Tingus K, Khoo T, Thompson PM, Bartzokis G. Age-related slowing in cognitive processing speed is associated with myelin integrity in a very healthy elderly sample. J Clin Exp Neuropsychol. 2011; 33:1059–1068.10.1080/13803395.2011.595397 [PubMed: 22133139]

Madden DJ, Bennett IJ, Burzynska A, Potter GG, Chen NK, Song AW. Diffusion tensor imaging of cerebral white matter integrity in cognitive aging. Biochim Biophys Acta. 2012; 1822:386–400.10.1016/j.bbadis.2011.08.003 [PubMed: 21871957]

Oldfield RC. The assessment and analysis of handedness: The Edinburgh inventory. Neuropsychologia. 1971; 9:97–113. [PubMed: 5146491]

Paus T. Growth of white matter in the adolescent brain: Myelin or axon? Brain Cogn. 2010; 72:26–35. [PubMed: 19595493]

Paus T, Pesaresi M, French L. White matter as a transport system. Neuroscience. 2014; 276:117–125. [PubMed: 24508743]

Peters A. Structural changes in the normally aging cerebral cortex of primates. Prog Brain Res. 2002; 136:455–465. [PubMed: 12143402]

Pfefferbaum A, Rosenbloom MJ, Chu W, Sassoon SA, Rohlfing T, Pohl KM, Zahr NM, Sullivan EV. White matter microstructural recovery with abstinence and decline with relapse in alcohol dependence interacts with normal ageing: A controlled longitudinal DTI study. The Lancet Psychiatry. 2014; 1:202–212. [PubMed: 26360732]

Pfefferbaum A, Sullivan EV. Cross-sectional versus longitudinal estimates of age-related changes in the adult brain: Overlaps and discrepancies. Neurobiol Aging. 201510.1016/j.neurobiolaging.2015.05.005

Pickering TG, Hall JE, Appel LJ, Falkner BE, Graves J, Hill MN, Jones DW, Kurtz T, Sheps SG, Roccella EJ. Recommendations for blood pressure measurement in humans and experimental animals: Part 1: Blood pressure measurement in humans: A statement for professionals from the subcommittee of professional and public education of the American Heart Association Council on High Blood Pressure Research. Hypertension. 2005; 45:142–161.10.1161/01.HYP.0000150859.47929.8e [PubMed: 15611362]

R Core Team. R: A language and environment for statistical computing. Vienna, Austria: R Foundation for Statistical Computing; 2014. Retrieved from http://www.R-project.org/

Radloff LS. The CES-D scale: A self-report depression scale for research in the general population. Appl Psychol Meas. 1977; 1:385–401.10.1177/014662167700100306

Raz, N. Aging of the brain and its impact on cognitive performance: Integration of structural and functional findings. 2000.

Raz, N. Encyclopedia of Life Sciences. London: Nature Publishing Group; Oct. 2001 Ageing and the Brain. http://www.els.net/doi:10.1038/npg.els.0003375

Raz N, Ghisletta P, Rodrigue KM, Kennedy KM, Lindenberger U. Trajectories of brain aging in middle-aged and older adults: Regional and individual differences. Neuroimage. 2010; 51:501–511.10.1016/j.neuroimage.2010.03.020 [PubMed: 20298790]

Raz, N.; Kennedy, K. A systems approach to age-related change: Neuroanatomical changes, their modifiers, and cognitive correlates. In: Jagust, W.; D'Esposito, M., editors. Imaging the aging brain. Oxford University Press; New York, NY: 2009. p. 43-70.

Raz N, Lindenberger U, Rodrigue KM, Kennedy KM, Head D, Williamson A, Dahle C, Gerstorf D, Acker JD. Regional brain changes in aging healthy adults: General trends, individual differences and modifiers. Cereb Cortex. 2005; 15:1676–1689.10.1093/cercor/bhi044 [PubMed: 15703252]

Raz N, Rodrigue K. Differential aging of the brain: Patterns, cognitive correlates and modifiers. Neurosci Biobehav Rev. 2006; 30:730–748.10.1016/j.neubiorev.2006.07.001 [PubMed: 16919333]

Raz N, Rodrigue KM, Kennedy KM, Acker JD. Vascular health and longitudinal changes in brain and cognition in middle-aged and older adults. Neuropsychology. 2007; 21:149–157. [PubMed: 17402815]

Raz N, Yang YQ, Rodrigue KM, Kennedy KM, Lindenberger U, Ghisletta P. White matter deterioration in 15 months: Latent growth curve models in healthy adults. Neurobiol Aging. 2012; 33:429e421, 425.10.1016/j.neurobiolaging.2010.11.018 [PubMed: 21194799]

Reisberg B, Franssen EH, Hasan SM, Monteiro I, Boksay I, Souren LE, Kenowsky S, Auer SR, Elahi S, Kluger A. Retrogenesis: Clinical, physiologic, and pathologic mechanisms in brain aging, Alzheimer's and other dementing processes. Eur Arch Psychiatry Clin Neurosci. 1999; 249:S28–S36.

Sadeghi N, Prastawa M, Fletcher PT, Wolff J, Gilmore JH, Gerig G. Regional characterization of longitudinal DT-MRI to study white matter maturation of the early developing brain. Neuroimage. 2013; 68:236–247.10.1016/j.neuroimage.2012.11.040 [PubMed: 23235270]

Sandell JH, Peters A. Disrupted myelin and axon loss in the anterior commissure of the aged rhesus monkey. The Journal of comparative neurology. 2003; 466:14–30. [PubMed: 14515238]

Sexton CE, Walhovd KB, Storsve AB, Tamnes CK, Westlye LT, Johansen-Berg H, Fjell AM. Accelerated changes in white matter microstructure during aging: A longitudinal diffusion tensor imaging study. J Neurosci. 2014; 34:15425–15436.10.1523/JNEUROSCI.0203-14.2014 [PubMed: 25392509]

Simmonds DJ, Hallquist MN, Asato M, Luna B. Developmental stages and sex differences of white matter and behavioral development through adolescence: A longitudinal diffusion tensor imaging (DTI) study. Neuroimage. 2014; 92:356–368.10.1016/j.neuroimage.2013.12.044 [PubMed: 24384150]

Smith SM, Jenkinson M, Johansen-Berg H, Rueckert D, Nichols TE, Mackay CE, Watkins KE, Ciccarelli O, Cader MZ, Matthews PM, Behrens TE. Tract-based spatial statistics: Voxelwise analysis of multi-subject diffusion data. Neuroimage. 2006; 31:1487–1505.10.1016/j.neuroimage.2006.02.024 [PubMed: 16624579]

Song SK, Sun SW, Ju WK, Lin SJ, Cross AH, Neufeld AH. Diffusion tensor imaging detects and differentiates axon and myelin degeneration in mouse optic nerve after retinal ischemia. Neuroimage. 2003; 20:1714–1722. [PubMed: 14642481]

Song SK, Sun SW, Ramsbottom MJ, Chang C, Russell J, Cross AH. Dysmyelination revealed through MRI as increased radial (but unchanged axial) diffusion of water. Neuroimage. 2002; 17:1429–1436. [PubMed: 12414282]

Song SK, Yoshino J, Le TQ, Lin SJ, Sun SW, Cross AH, Armstrong RC. Demyelination increases radial diffusivity in corpus callosum of mouse brain. Neuroimage. 2005; 26:132–140.10.1016/j.neuroimage.2005.01.028 [PubMed: 15862213]

Sullivan EV, Adalsteinsson E, Hedehus M, Ju C, Moseley M, Lim KO, Pfefferbaum A. Equivalent disruption of regional white matter microstructure in ageing healthy men and women. Neuroreport. 2001; 12:99. [PubMed: 11201100]

Sullivan EV, Rohlfing T, Pfefferbaum A. Quantitative fiber tracking of lateral and interhemispheric white matter systems in normal aging: Relations to timed performance. Neurobiol Aging. 2010; 31:464–481.10.1016/j.neurobiolaging.2008.04.007 [PubMed: 18495300]

Sullivan EV, Rohlfing T, Pfefferbaum A. Longitudinal study of callosal microstructure in the normal adult aging brain using quantitative DTI fiber tracking. Dev Neuropsychol. 2010; 35:233–256.10.1080/87565641003689556 [PubMed: 20446131]

Sun SW, Liang HF, Cross AH, Song SK. Evolving Wallerian degeneration after transient retinal ischemia in mice characterized by diffusion tensor imaging. Neuroimage. 2008; 40:1–10. [PubMed: 18187343]

Sun SW, Liang HF, Le TQ, Armstrong RC, Cross AH, Song SK. Differential sensitivity of in vivo and ex vivo diffusion tensor imaging to evolving optic nerve injury in mice with retinal ischemia. Neuroimage. 2006; 32:1195–1204. [PubMed: 16797189]

Sun SW, Neil JJ, Song SK. Relative indices of water diffusion anisotropy are equivalent in live and formalin- fixed mouse brains. Magn Reson Med. 2003; 50:743–748. [PubMed: 14523960]

Takao H, Hayashi N, Kabasawa H, Ohtomo K. Effect of scanner in longitudinal diffusion tensor imaging studies. Hum Brain Mapp. 2012; 33:466–477.10.1002/hbm.21225 [PubMed: 21391276]

Teipel SJ, Meindl T, Wagner M, Stieltjes B, Reuter S, Hauenstein KH, Filippi M, Ernemann U, Reiser MF, Hampel H. Longitudinal changes in fiber tract integrity in healthy aging and mild cognitive

impairment: A DTI follow-up study. Journal of Alzheimer's disease : JAD. 2010; 22:507–522.10.3233/JAD-2010-100234 [PubMed: 20847446]

Vargas ME, Barres BA. Why is Wallerian degeneration in the CNS so slow? Annu Rev Neurosci. 2007; 30:153–179. [PubMed: 17506644]

Vernooij MW, de Groot M, van der Lugt A, Ikram MA, Krestin GP, Hofman A, Nielsen WJ, Breteler MM. White matter atrophy and lesion formation explain the loss of structural integrity of white matter in aging. Neuroimage. 2008; 43:470–477.10.1016/j.neuroimage.2008.07.052 [PubMed: 18755279]

Vernooij MW, Ikram MA, Vrooming HA, Wielopolski PA, Krestin GP, Hofman A, Niessen WJ, Van der Lugt A, Breteler MM. White matter microstructural integrity and cognitive function in a general elderly population. Arch Gen Psychiatry. 2009; 66:545–553.10.1001/archgenpsychiatry.2009.5 [PubMed: 19414714]

Vik A, Hodneland E, Haasz J, Ystad M, Lundervold AJ, Lundervold A. Fractional anisotropy shows differential reduction in frontal-subcortical fiber bundles-a longitudinal MRI study of 76 middle-aged and older adults. Front Aging Neurosci. 2015; 7:81.10.3389/fnagi.2015.00081 [PubMed: 26029102]

Wang SS, Shultz JR, Burish MJ, Harrison KH, Hof PR, Towns LC, Wagers MW, Wyatt KD. Functional trade-offs in white matter axonal scaling. J Neurosci. 2008; 28:4047–4056.10.1523/JNEUROSCI.5559-05.2008 [PubMed: 18400904]

Zahr NM, Rohlfing T, Pfefferbaum A, Sullivan EV. Problem solving, working memory, and motor correlates of association and commissural fiber bundles in normal aging: A quantitative fiber tracking study. Neuroimage. 2009; 44:1050–1062.10.1016/j.neuroimage.2008.09.046 [PubMed: 18977450]

Zhang YY, Brady M, Smith S. Segmentation of brain MR images through a hidden Markov random field model and the expectation-maximization algorithm. IEEE Trans Med Imaging. 2001; 20:45–57.10.1109/42.906424 [PubMed: 11293691]

Highlights

- White matter in healthy adults studied with DTI over 7 years, up to four occasions.
- Late developing white matter regions declined more than earlier developing regions.
- Association fibers showed the greatest decline with advanced age.
- Posterior limb of internal capsule appears less vulnerable to age-related decline.
- This findings support the last-in first-out hypothesis of brain aging.

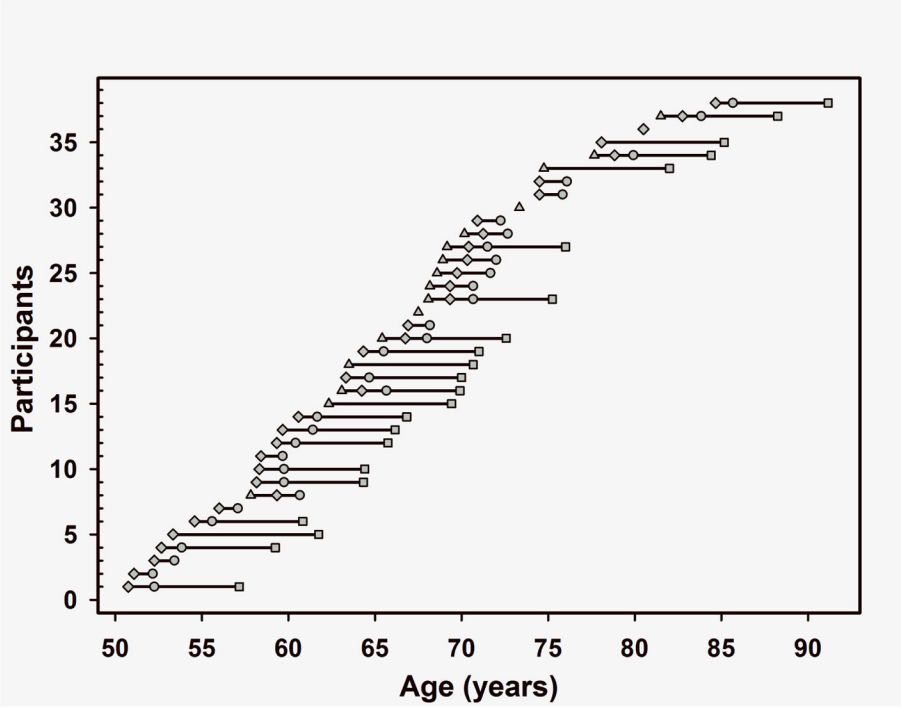

Figure 1.

Distribution of ages-at-measurement and intervals between measurement occasions for the 38 participants. Each row indicates a single participant, with lines denoting time between measurement occasions, and symbols representing each separate measurement occasion as follows: triangle = 1st occasion; diamond = 2nd occasion; circle = 3rd occasion; square = 4th occasion. See the Method section 2.1 for details on the differences in assessment intervals.

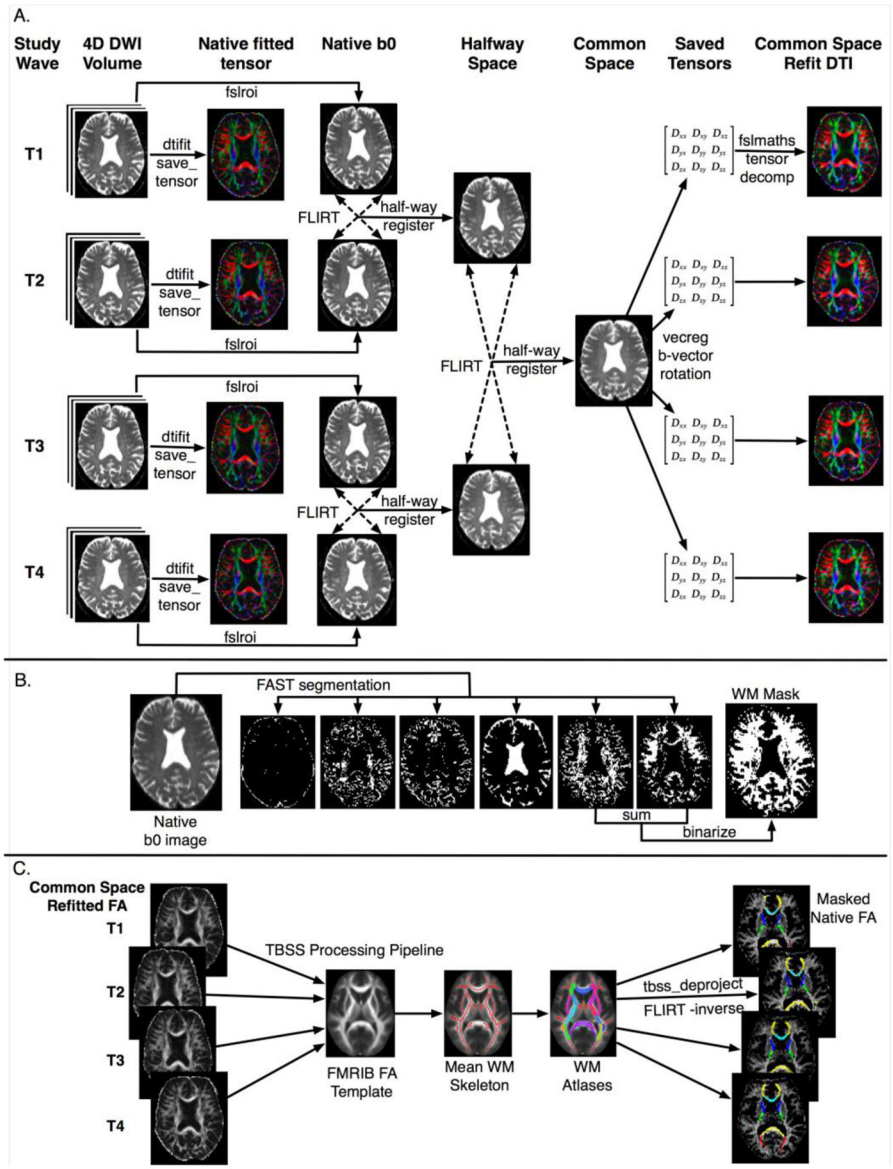

Figure 2.

DTI processing pipeline. A. Common space determination across all measurement occasions is performed using the non-diffusion weighted b0 images which are hierarchically registered using a 6-degree of freedom, rigid registration, first between waves 1–2 and waves 3–4 to determine halfway, common space between these images; the resulting halfway 1–2 and 3–4 image spaces are subsequently registered and the halfway space from these provides a final, common space between all images. Native space diffusion tensors are fit to the data using FSL's dtifit procedure, with the – save_tensor flag to retain the tensor components. Next, using the vecreg command in FSL, the saved tensor components are subsequently rotated and refit to the common space. B. Masking of white matter hyperintensities (WMH) and cerebrospinal fluid (CSF) is performed using FAST segmentation of the native b0 image into 6 classes based on voxel intensity. The two segmented masks that correspond primarily to WM are summed and binarized into a WM mask that omits areas of apparent WMH,

CSF, and image noise. C. The FA images that were refit into common space in A., above are used as the basis for TBSS processing which nonlinearly transforms the data into standard space, and registers them to the $1mm^3$ FMRIB58 FA image before calculating mean FA across the sample and determining a mean WM skeleton. Using the tbss_deproject routine and inverse transformation matrices from the initial registration steps the JHU WM labels and tractography atlases (Mori et al., 2005; Wakana et al., 2007) are subsequently transformed back to individual native space, but are confined to the mean WM skeleton. Individual ROIs from the atlas are segmented and the DTI maps (FA, AD, RD), masked for WMH/CSF are sampled from those regions across participants.

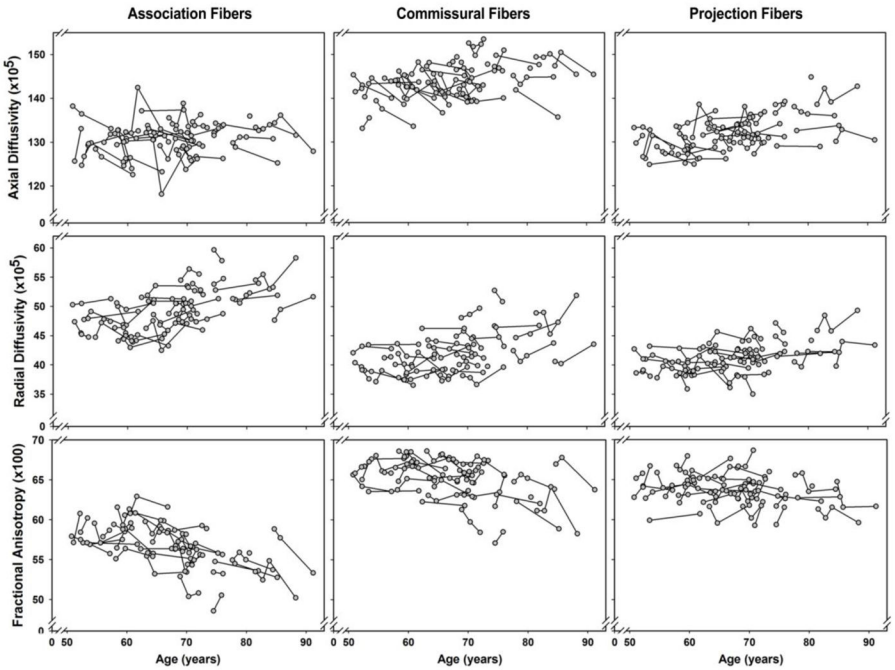

Figure 3.

Longitudinal changes over 1 to 4 occasions of measurement. The plots are organized by three fiber types (columns, left to right): Association, commissural, and projection fiber regions, and by three indices of WM micro-organization (rows, top to bottom): Axial diffusivity, radial diffusivity, and fractional anisotropy.

Table 1

Participant characteristics

Baseline Variables	Women Mean (SD)	Men Mean (SD)	*t* or χ^{2a}	*p*
Age (years)	63.85 (8.91)	67.31 (8.98)	1.19	.244
MMSE	28.43 (1.08)	28.71 (1.36)	0.70	.487
Education (years)	16.14 (2.67)	17.71 (2.20)	1.99	.054
Systolic BP (mmHg)	128.00 (10.82)	131.52 (12.29)	0.94	.355
Diastolic BP (mmHg)	78.71 (7.45)	75.97 (7.67)	1.11	.272
% Smokers	0.0%	11.77%	2.61[1]	.106
% Exercise	80.95%	64.71%	1.28	.258
Days Exercise /Week	3.41 (2.46)	2.79 (2.42)	0.77	.449
% Hypertension Dx	28.57%	35.29%	0.20	.658

Notes: SD=standard deviation;

[1] *a* = single degree of freedom chi-square test; BP=blood pressure; Dx=diagnosis

Table 2

Results from Linear Mixed Effects Models

Fixed Effects	Estimate	Std. Error	df	t value	Pr(>|t|)
			Axial Diffusivity		
Intercept (Association Fibers)	129.496	5.313	9.202	24.374	0.000
Time (centered at 70)	−0.378	0.056	1189.405	−6.700	0.000
Initial Age (centered at 65.4)	0.481	0.070	183.242	6.865	0.000
Projection Fibers	1.783	9.885	9.002	0.180	0.861
Commissural Fibers	13.471	7.472	9.002	1.803	0.105
High Blood Pressure	2.226	0.917	35.956	2.426	0.020
Time × Initial Age	−0.001	0.004	84.144	−0.178	0.859
Time × Projection Fibers	0.173	0.041	1160.311	4.219	0.000
Time × Commissural Fibers	0.113	0.031	1160.311	3.663	0.000
			Radial Diffusivity		
Intercept (Association Fibers)	48.337	3.194	9.586	15.135	0.000
Time (centered at 70)	0.093	0.031	1167.389	3.040	0.002
Initial Age (centered at 65.4)	0.148	0.058	57.715	2.560	0.013
Projection Fibers	−8.386	5.881	9.002	−1.426	0.188
Commissural Fibers	−7.562	4.446	9.002	−1.701	0.123
High Blood Pressure	2.052	1.006	32.539	2.040	0.050
Time × Initial Age	0.012	0.003	321.887	4.303	0.000
Time × Projection Fibers	−0.087	0.022	1156.537	−3.927	0.000
Time × Commissural Fibers	−0.033	0.017	1156.537	−1.948	0.052
			Fractional Anisotropy		
Intercept (Association Fibers)	57.134	3.730	9.242	15.318	0.000
Time (centered at 70)	−0.163	0.029	1172.908	−5.646	0.000
Initial Age (centered at 65.4)	−0.008	0.046	75.489	−0.181	0.857
Projection Fibers	7.304	6.932	9.001	1.054	0.319
Commissural Fibers	8.525	5.240	9.001	1.627	0.138
High Blood Pressure	−1.182	0.743	32.098	−1.591	0.121

Fixed Effects	Estimate	Std. Error	df	t value	Pr(>|t|)
Time × Initial Age	−0.008	0.002	182.345	−3.482	0.001
Time × Projection Fibers	0.104	0.021	1156.103	5.008	0.000
Time × Commissural Fibers	0.049	0.016	1156.103	3.090	0.002

Note: REML was used for parameter estimation. Variance of random effects for (a) Axial diffusivity: Var(ζ_i), = 5.36, Var(ζ_j) = 139.37, Var(ε_{ijt}) = 20.12; (b) Radial diffusivity: Var(ζ_i), = 7.19, Var(ζ_j) = 49.35, Var(ε_{ijt}) = 5.87; (c) Fractional anisotropy: Var(ζ_i), = 3.84, Var(ζ_j) = 68.59, Var(ε_{ijt}) = 5.19. Variance of random effects were tested using ML likelihood ratio tests.